EXAFS spectroscopy on overpressurized krypton bubbles in copper and nickel

1997 J. Phys.: Condens. Matter 9 149

(http://iopscience.iop.org/0953-8984/9/1/016)

J. Phys.: Condens. Matter **9** (1997) 149–155. Printed in the UK PII: S0953-8984(97)77106-6

EXAFS spectroscopy on overpressurized krypton bubbles in copper and nickel

M F Rosu†, L Niesen†, A van Veen† and J H Evans‡

† Materials Science Centrum, Nijenborgh 4, 9747 AG Groningen, The Netherlands

‡ Department of Physics, Royal Holloway, University of London, Egham TW20 0EX, UK

Received 12 August 1996

Abstract. Bulk copper and nickel samples containing 2.5 and 5 at.% krypton present in overpressurized bubbles have been studied by EXAFS spectroscopy. A fit to the experimental data yields krypton nearest-neighbour distances of 3.62(4) and 3.69(4) Å in a copper and a nickel matrix respectively. These values confirm that krypton bubbles are overpressurized. Calculated krypton packing densities are in good agreement with results from other techniques. In addition, average krypton–metal nearest-neighbour distances of 3.0(1) Å were determined. Atomistic calculations show a wide variation of krypton–metal distances, in agreement with the experiment.

1. Introduction

The behaviour of krypton in metals has attracted interest over the past decade, from both the fundamental and applied points of view. The applied interest was initiated by Whitmell and co-workers [1, 2] who responded to the potential problem of disposing of radioactive ^{85}Kr (a by-product of nuclear fuel processing) by developing a combined ion implantation deposition and sputtering technique to immobilize the krypton in either copper or nickel. Meanwhile, considerable fundamental interest has arisen from the discovery in 1984 that the heavier inert gases can precipitate even at ambient temperatures in the solid phase in metals [3, 4]. This general area is covered by several articles in a recent review volume [5].

While relatively thin near-surface layers of high inert gas concentrations can be achieved in metals by ion implantation, one attractive outcome of applied interest was the production of samples of both copper and nickel, with thicknesses of the order of one centimetre, having uniform krypton concentrations of a few atomic per cent. The samples are built up layer by layer, alternately adding material by sputter deposition and implanting krypton ions with energies up to 3 keV using a glow discharge. Clearly the gas deposition process is accompanied by considerable radiation damage. Nevertheless, the production of these effectively bulk samples has allowed the application of more techniques to study inert gas precipitation in metals. In particular both the Cu–Kr and Ni–Kr materials have been studied with positron spectroscopy [6, 7] and small-angle neutron scattering [7]. The present EXAFS study adds to these techniques.

Basic information on the underlying structures in Cu–Kr and Ni–Kr has been obtained by conventional transmission electron microscopy (TEM) and electron diffraction techniques. TEM observations of as-deposited materials revealed a structure of randomly oriented metal

0953-8984/97/010149+07$19.50

grains of about 0.2–0.3 μm and within these grains a high density of krypton bubbles with diameters ranging up to 2 nm. In the past there have been several discussions [6, 8, 9] on the fraction of gas contained in the bubbles visible by TEM. TEM data [9] suggested this fraction could be as low as 25% leaving the remainder to be present in submicroscopic bubbles and Kr–vacancy clusters. Lattice parameter measurements [8] and detailed positron annihilation spectroscopy (PAS) [6] support the overall picture of krypton association with vacancies over the size range from the visible bubbles down to the simplest Kr–vacancy combinations. Considering the conditions of preparation, this wide range of complexes is not too surprising. However, there is considerable uncertainty on the actual size distribution of complexes.

More definite information is available on the krypton residing in the bubbles. Electron diffraction measurements showed that the krypton is present in the solid phase with an FCC structure and with packing densities of 2.9 and 3.2×10^{28} m^{-3} in Cu–Kr and Ni–Kr respectively [10]. These numbers apply to the smallest bubbles observed in the electron microscope, and correspond to lattice constants of 5.2 and 5.0 Å respectively. From density measurements values of 3.2 and 2.8×10^{28} m^{-3} have been derived for Cu–Kr and Ni–Kr materials respectively [8].

Complementary information on the solid phase bubbles is also available from several PAS investigations [6, 7]. It is quite clear [11, 12] that the krypton–metal interface acts as a trap for positrons while the positron lifetime is a measure of the density of Kr in the bubbles. The values found for the packing densities, 2.6–2.9 and 2.8–2.9 $\times 10^{28}$ m^{-3} for Cu–Kr and Ni–Kr respectively, are in reasonable agreement with earlier results [6].

EXAFS spectroscopy offers the possibility to obtain information about the local structure around isolated atoms or clusters of atoms randomly distributed in a host matrix. In this paper we investigate the potential of the technique to give further information on the complex state of krypton in the Cu–Kr and Ni–Kr materials. From the determined nearest-neighbour distance, the packing density of krypton can be deduced and compared with values obtained from other techniques. Also information about the number of nearest neighbours and their type can be inferred from an EXAFS spectrum. It is important to note that the derived nearest-neighbour distance is an average over all Kr atoms in the sample.

2. Experimental results and discussion

The measurements were performed at beam station 9.2 of the Synchrotron Radiation Source at Daresbury. A parallel double-crystal spectrometer consisting of two (220) Si crystals was used as a monochromator. The positions of the monochromator were set such that the energies of the incoming photons ranged between 14 and 14.7 keV. Higher-harmonic rejection was accomplished by slightly mistuning the two crystals.

Several K-edge spectra have been taken for krypton immobilized in both copper and nickel host materials. The Cu–Kr sample contained 2.5–3 at.% Kr, while the Ni–Kr sample contained approximately 5 at.%. The measurements were performed at a temperature of 85 K. The fluorescence yield was measured with twelve Ge detectors placed in such a way that a large solid angle was covered. The total fluorescence spectrum is the sum of the twelve individual fluorescence spectra divided by the intensity of the incoming beam as measured by an ion chamber.

Figure 1 illustrates the EXAFS spectrum for krypton in a nickel matrix. The spectrum for krypton in copper is very similar. It can be observed that the fine structure of the post-edge region has a small amplitude and is very strongly damped. It practically disappears at about 150 eV above the K edge. Because of this, no k dependent weighting was applied

to the spectrum obtained after background subtraction. The EXCURV92 [13] program was used to fit the experimental data. The photoelectron was described by the curved wave theory. The ground state energy was calculated according to the von Barth theory while the exchange energy was based on the Hedin–Lundqvist theory. The potentials and the phase shifts for each type of atom depend on its chosen neighbour. The theoretical fit is based on a three-shell structure around the excited Kr atom. The first shell has the smallest radius and it contains the metal neighbours; the second and the third shell contain krypton atoms and their radii are associated with the nearest- and next-nearest-neighbour distance respectively. This simple model neglects metal atoms at larger distances. This will introduce extra errors in the derived distances.

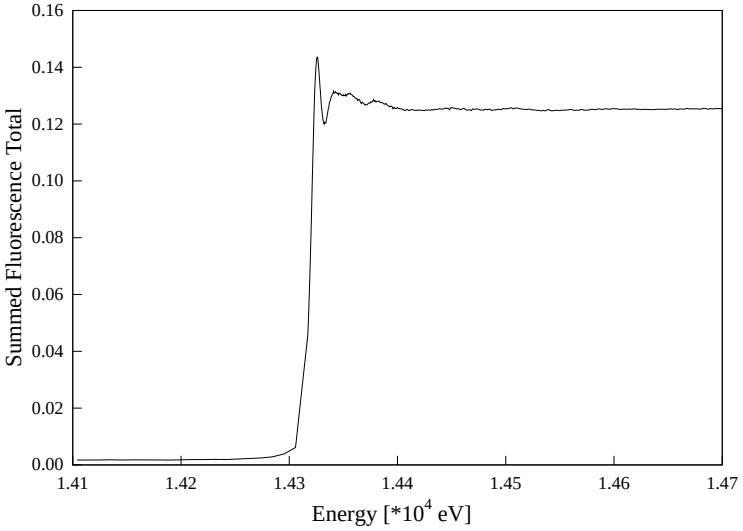

Figure 1. EXAFS spectrum of Kr incorporated in an Ni matrix.

The experimental EXAFS oscillations together with the theoretical fit are illustrated in figures 2 and 3. The determined radii of the three shells for both measurements are included in table 1. The errors given are from the fit.

Table 1. Determined values for the krypton–metal distances, and the krypton nearest-neighbour and krypton next-nearest-neighbour distances for Kr clusters in copper and nickel.

Material	Kr–metal (Å)	Kr nearest neighbour (Å)	Kr next-nearest neighbour (Å)
Cu–Kr	3.0(1)	3.62(4)	5.33(6)
Ni–Kr	3.0(1)	3.69(4)	5.09(8)

As already discussed in the introduction, a distribution in bubble size and maybe in krypton densities is present in these materials. The bubbles may be bounded by several planes with different orientations such that different edge sites of the krypton atoms may lead to a broad distribution in the krypton–metal nearest-neighbour distance. Also a distribution in krypton nearest-neighbour and next-nearest-neighbour distances may be present. Therefore, the determined values for these distances have to be interpreted as average values.

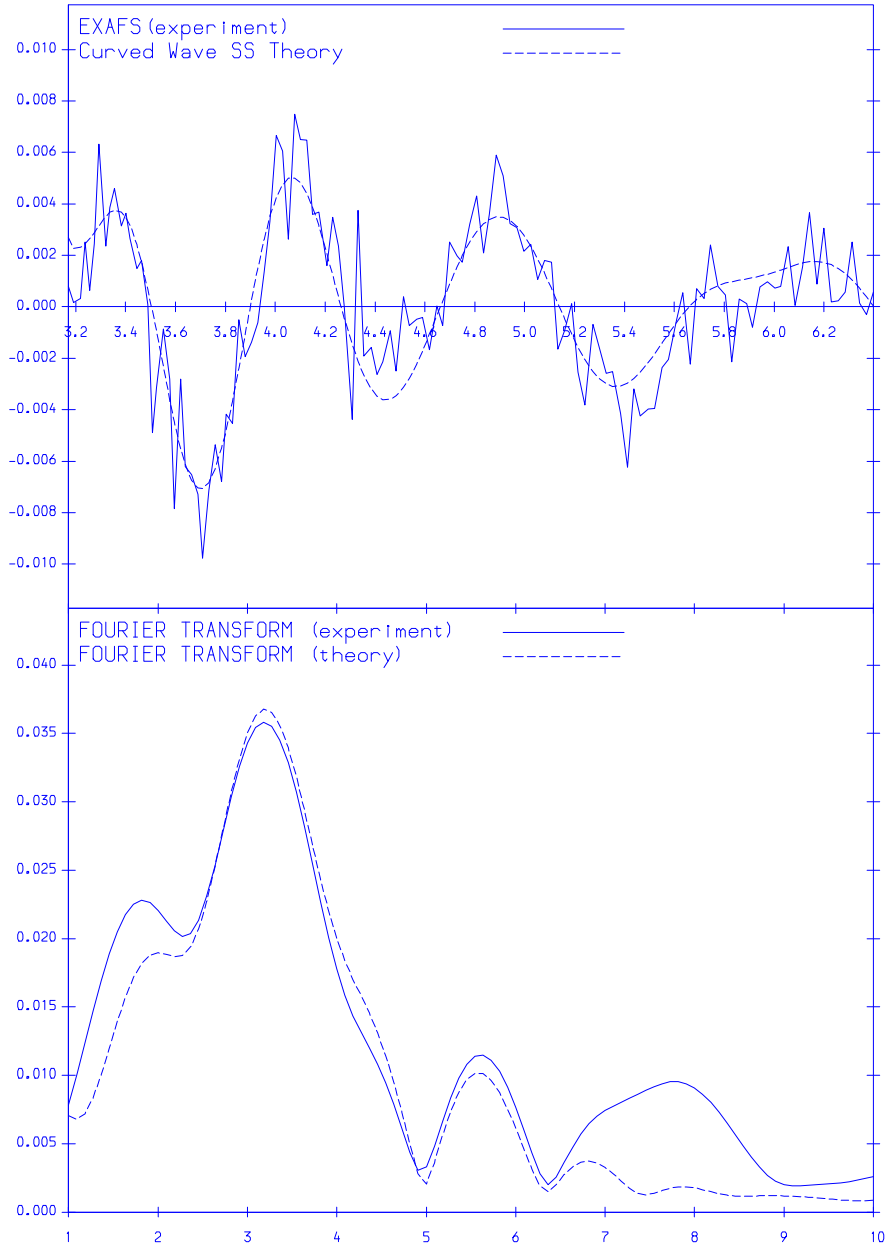

Figure 2. EXAFS oscillations after background subtraction together with the Fourier transform for the Kr–Cu sample.

On average 1.2(4) metal atoms are present in the first shell, while the number of krypton nearest neighbours is about 9.6, implying that the bulk fraction is larger than the interface fraction. This is in agreement with a relatively small number of isolated krypton atoms or small Kr–vacancy clusters.

The nearest-neighbour distance for solid krypton at 1 atm and RT is 4.04 Å. The values

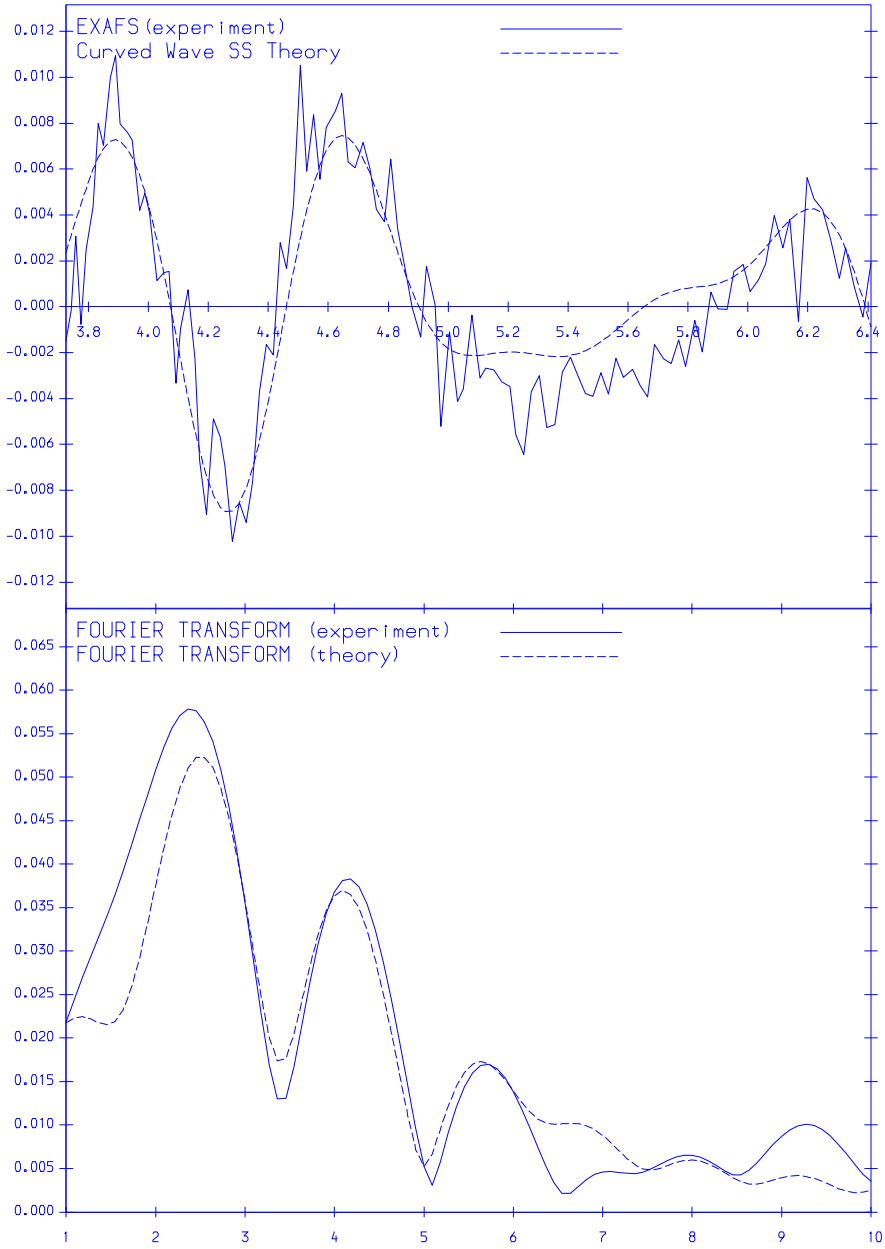

Figure 3. EXAFS oscillations after background subtraction and the Fourier transform for Kr–Ni.

found in this experiment are smaller and this evidences the fact that krypton bubbles are overpressurized.

The next-nearest-neighbour distances determined for krypton in both metallic matrices are also smaller than the values for solid krypton at 1 atm: 5.33(6) Å in a Cu matrix and 5.09(8) Å in an Ni matrix. These values would give nearest-neighbour distances of 3.77(4) Å and 3.60(4) Å for krypton in a Cu and in an Ni matrix respectively.

An average nearest-neighbour distance can be calculated. This gives 3.70 Å in Cu and 3.65 Å in Ni and these two values are not significantly different. The corresponding molar volumes are 21.6 and 20.7 cm^3. Although measured at 85 K, we expect the same values at room temperature because the accessible volume is given by the metallic matrix whose thermal expansion is negligible between 85 and 300 K. The equation of state (EOS) for Kr yields a pressure in the precipitate of 2.1 GPa at 85 K [14] which increases to ∼3.6 GPa at 295 K [15].

The corresponding krypton packing densities are 2.8(1) and $2.9(1) \times 10^{28}$ m^{-3} in a Cu and an Ni matrix respectively. The agreement with earlier results is quite good considering that different samples were used for different measurements. It also implies that the Kr atoms which escaped detection in electron microscopy do not have significantly lower nearest-neighbour distances than the Kr atoms that contribute to electron diffraction. This supports the assumption that these Kr atoms reside in precipitates that are just too small to be observed by TEM.

At this point it may be instructive to calculate the variation in the metal atom radii when a local stress of 3–6 GPa is present. The radii of a Cu and an Ni atom at normal pressure are 1.28 and 1.25 Å respectively, while their bulk moduli are 1.374 and 1.86×10^{11} N m^{-2}. A calculation yields a variation of the radius of 0.009 up to 0.02 Å for a Cu atom and 0.006 up to 0.013 Å for an Ni atom. This shows that the radii of the metal atoms will not change considerably even when a very high local stress is present.

Atomistic calculations on krypton–vacancy defect clusters varying in size from Kr_2V_6 up to $Kr_{171}V_{665}$ in nickel microcrystallites containing 3848 atoms have also been performed. The largest bubble was cuboidally shaped. The temperature was kept at 0 K. Thus, no thermal motion or thermal expansion was taken into account, but this is in agreement with the fact that we do not expect a significant lattice expansion and that the bubble volume is determined by the metallic lattice and is constant. The atom embedding scheme of Finnis and Sinclair [16] was used to describe the Ni–Ni interaction potential. The Kr–Kr potential was described by a Born–Mayer exponential potential $V(r) = A \exp(-br)$ with values $A = 1.2 \times 10^6$ eV and $b = 5.15$ $Å^{-1}$ by fitting to the Barker potential [17]. The Kr–Ni potential was derived by a scheme given by Wilson *et al* [18].

The packing density of the krypton in the largest simulated bubble was determined to be 3.5×10^{28} m^{-3} which corresponds to a pressure of 6.4 GPa. For lower packing densities the Kr–Kr nearest-neighbour distance was found to be 3.65 Å at a pressure of 2.06 GPa which is in agreement with the experimental values.

Regarding the Kr–Ni interaction distances we found that the separation between adjacent Kr and Ni (100) planes of the largest bubble amounted to 3.2 Å, implying that the Kr–Ni nearest-neighbour distances are even larger. For additional Ni atoms filling the corner of the cubic bubble, the Kr–Ni distances became 3.12 Å. For the Kr_2V_6 cluster the minimum Kr–Ni distances amounted to 2.76 Å. We can conclude from the calculations that the Kr–Ni distances vary appreciably depending on the size of the bubble and the local configuration. This is in line with the experimental observation of a broad distribution of Kr–Ni distances.

3. Conclusions

Cu–Kr and Ni–Kr materials have been intensively studied. The overall structure of the as-deposited materials as determined from several different techniques consists of a random distribution of microscopic and submicroscopic overpressurized krypton bubbles having packing densities of about $2.8–2.9 \times 10^{28}$ m^{-3}. EXAFS measurements confirm this global picture and give krypton nearest-neighbour distances, and consequently packing densities,

which agree with previous results. From the low average number of metal neighbours we conclude that the amount of krypton present as isolated atoms or small vacancy clusters is small. The observed average krypton–metal distances are in reasonable agreement with the atomistic calculations, which show also a large variation in these distances.

Acknowledgment

One of the authors, J H Evans, thanks the Leverhulme Trust for the receipt of a travel grant during the course of this work.

References

[1] Whitmell D S 1982 *Nucl. Energy* **21** 181
[2] Whitmell D S, Nelson R S, Williamson R, Smith M J S and Bauer G J 1983 *Eur. Appl. Res. Rep. Nucl. Sci. Technol.* **5** 513
[3] Templier C, Jaouen C, Riviere J-P, Delafond J and Grilhe J 1984 *C. R. Acad. Sci. Paris* **299** 613
[4] vom Felde A, Fink J, Muller-Heeinzering Th, Pfluger J, Scheerer B, Linker G and Kalleta D 1984 *Phys. Rev. Lett.* **53** 922
[5] Donnelly S E and Evans J H (ed) 1991 *Fundamental Aspects of Inert Gases in Solids (NATO ASI Series B: Physics 279)* (New York: Plenum)
[6] Jensen K O, Eldrup M, Pedersen N J and Evans J H 1988 *J. Phys. F: Met. Phys.* **18** 1703
[7] Eldrup M, Skov Jensen J, Horswell A, Jensen K O and Evans J H 1983 *Eur. Appl. Res. Rep. Nucl. Sci. Technol.* **5** 221
[8] Evans J H, Williamson R and Whitmell D S 1985 *Efects of Radiation on Materials: 12th Int. Symp.* ASTM STP870, ed A Garner and J S Perrin (Philadelphia, PA: American Society for Testing and Materials) p 1225
[9] Eldrup M and Evans J H 1982 *J. Phys F: Met. Phys.* **12** 1265
[10] Evans J H and Mazey D J 1985 *J. Phys. F: Met. Phys.* **15** L1
[11] Jensen K O and Nieminen R M 1987 *Phys. Rev.* B **35** 2087
[12] Jensen K O and Nieminen R M 1987 *Phys. Rev.* B **36** 8219
[13] Binstead N, Campbell J W, Gurman S J and Stephenson P C 1991 *SERC Daresbury Laboratory EXCURV92 Program*
[14] Anderson M S and Swenson C A 1975 *J. Phys. Chem. Solids* **36** 145
[15] Polian A, Besson J M, Grimsditch M and Grosshans W A 1989 *Phys. Rev.* B **39** 1332
[16] Finnis M W and Sinclair J E 1984 *Phil. Mag.* A **50** 45
[17] Barker J A, Watts R O, Lee J K, Schafer T P and Lee Y T 1974 *J. Chem. Phys.* **61** 3081
[18] Wilson W D and Bisson C L 1971 *Phys. Rev.* B **3** 3984